

Concept Drift Detection for Imbalanced Stream Data

Heng Wang
 Johns Hopkins University
 Email: hwang82@jhu.edu

Zubin Abraham
 Bosch Research North America
 Email: Zubin.Abraham@us.bosch.com

Abstract—Common statistical prediction models often require and assume stationarity in the data. However, in many practical applications, changes in the relationship of the response and predictor variables are regularly observed over time, resulting in the deterioration of the predictive performance of these models. This paper presents Linear Four Rates (LFR), a framework for detecting these concept drifts and subsequently identifying the data points that belong to the new concept (for relearning the model). Unlike conventional concept drift detection approaches, LFR can be applied to both batch and stream data; is not limited by the distribution properties of the predictor variable (e.g., datasets with imbalanced labels); is independent of the underlying statistical-model; and uses user-specified parameters that are intuitively comprehensible. The performance of LFR is compared to benchmark approaches using both simulated and commonly used public datasets that span the gamut of concept drift types. The results show LFR significantly outperforms benchmark approaches in terms of recall, accuracy and delay in detection of concept drifts across datasets.

I. INTRODUCTION

A common challenge when mining data streams is that the data streams are not always strictly stationary, i.e., the concept of data (underlying distribution of incoming data) unpredictably drifts over time. This has encouraged the need to detect these concept drifts in the data streams in a timely manner, be it for business intelligence or as a means to track the performance of statistical prediction models that use these data streams as input.

This paper focuses on detecting concept drifts affecting binary classification models. For a binary classification problem, concept drift is said to occur when the joint distribution $P(\mathbf{X}_t, y_t)$ changes over time where $\mathbf{X}_t \in \mathbb{R}^d$ are the d predictor variables at time step t and $y_t \in \{0, 1\}$ the corresponding binary response variable. Intuitively, concept drift refers to the scenario when the underlying distribution that generates the response variable changes over time. Popular approaches for detecting concept drift identify the change point [1], [2]. DDM is the most widely used concept drift detection algorithm, that is strictly designed for streaming data [1]. The test statistic DDM employs is the sum of overall classification error (\hat{P}_{error}) and its empirical standard deviation (\hat{S}_{error}). DDM focuses on the overall error rate and hence fails to detect a drift unless the sum of false positive and false negatives changes. An example of such a scenario, is when a 2×2 confusion matrix changes from $\begin{pmatrix} 65 & 5 \\ 15 & 15 \end{pmatrix}$ to $\begin{pmatrix} 75 & 15 \\ 5 & 5 \end{pmatrix}$, thus preserving their overall error rate. This limitation is accentuated in imbalanced classification tasks [2], as seen in the example. Unfortunately, this failure to detect a drastic drop in recall of the minority class is often critical. For instance,

if the minority class in the above example corresponded to products at a manufacturing plant that were classified as defective, this critical threefold decrease in 'true positive rate' (i.e., from 0.75 to 0.25) would go unnoticed by DDM.

Drift Detection Method for Online Class Imbalance (DDM-OCI) addresses the limitation of DDM when class ratio is imbalanced [2]. However, DDM-OCI triggers a number of false alarms due to an inherent weakness in the model. DDM-OCI assumes that the concept drift in an imbalanced classification task is indicated by the change of underlying true positive rate (i.e., minority-class recall). This hypothesis unfortunately does not consider the case when concept drift occurs without affecting the recall of the minority class. It can be shown that it is possible for concept to drift from an imbalanced class data to balanced class data, while true positive rate (tpr), positive predicted value (ppv) and F1-score remain unchanged. Thus, this type of drift is unlikely to be detected by DDM-OCI unless other rates such as true negative rate (tnr) or negative predicted value (npv) are also considered. Additionally, the test statistic used by DDM-OCI $R_{tpr}^{(t)}$ is not approximately distributed as $\mathcal{N}(P_{tpr}, \frac{P_{tpr}(1 - P_{tpr})}{N_{tpr}})$, under the stable concept. Thus, the rationale of constructing confidence levels specified in [1] is not suitable with the null distribution of $R_{tpr}^{(t)}$. This is the reason DDM-OCI triggers false alarms quickly and frequently.

Early Drift Detection Method (EDDM) achieves better detection results than DDM if the data stream has slow gradual change. EDDM monitors the distance between the two classification errors [3]. PerfSim algorithm considers all the components of a confusion matrix and monitors the cosine similarity coefficient of all components from two batches of data [4]. If the similarity coefficient drops below some user-specified threshold, a concept drift is signified. However, both EDDM and PerfSim algorithms are constrained by the requirement for collecting batch data to calculate monitoring statistics. The method to partition data stream in [3], [4] is either user-specified by practical experience or to be learned before the start of detection. Hence, EDDM and PerfSim are not well suited for streaming environments. The approach specified in [5] makes use of SVM to monitor three measures: overall accuracy, recall, and precision over time. This approach too computes the three measures by assuming that the data arrives in batches, on which SVM is learned.

To address the limitations of existing approaches, we present Linear Four Rates (LFR) for detecting the drift of $P(\mathbf{X}_t, y_t)$. Unlike other proposed approaches, LFR can detect all possible variants of concept drift, even in the presence of imbalanced class labels, as shown in Section IV. LFR outperforms existing approaches in terms of earliest detection

of concept drift, with the least false alarms and best recall. Additionally, LFR does not require the data to arrive in batches and is independent of the underlying classifier employed.

II. PROBLEM FORMULATION

Given that detection of concept drift is equivalent to detecting a change-point in $P(\mathbf{X}_t, y_t)$, an intuitive approach is to test the statistical hypothesis upon the multivariate variable (\mathbf{X}_t, y_t) in the data stream [6], [7], [8]. The limitation of this approach is that the performance of the statistical power degrades when the dimension (d) of \mathbf{X}_t is extremely large or if the magnitude of the drift small. Hence, to overcome these limitations, the proposed approach identifies the change in $P(\hat{f}(\mathbf{X}_t), y_t)$ where \hat{f} is the classifier used for prediction. This is motivated by the fact that any drift of $P(\hat{f}(\mathbf{X}_t), y_t)$ would imply a drift in $P(\mathbf{X}_t, y_t)$, with probability 1.

Let $\hat{f}(\mathbf{X}_t) = \hat{y}_t$ be a binary classifier for the given data stream (\mathbf{X}_t, y_t) . We define the corresponding 2×2 confusion probability matrix (CP) for \hat{f} to be

| | | True | |
|------|---|------|----|
| | | 0 | 1 |
| Pred | 0 | TN | FN |
| | 1 | FP | TP |

where, $CP[1, 1]$, $CP[0, 0]$, $CP[1, 0]$, $CP[0, 1]$ denotes the underlying percentage of true positives (TP), true negatives(TN), false positives (FP) and false negatives (FN) respectively, for classifier \hat{f} . i.e., $CP[1, 1] = P(y_t = 1, \hat{y}_t = 1)$.

The four characteristic rates (True Positive Rate, True Negative Rate, Positive Predicted Value, Negative Predicted Value) can be computed as follows: $P_{tpr} = TP/(TP + FN)$, $P_{tnr} = TN/(TN + FP)$, $P_{ppv} = TP/(FP + TP)$ and $P_{npv} = TN/(TN + FN)$. All the mentioned characteristic rates in $P_\star = \{P_{tpr}, P_{tnr}, P_{ppv}, P_{npv}\}$ is equal to 1, if there is no misclassification.

Under a stable concept (i.e., $P(\mathbf{X}_t, y_t)$ remains unchanged), $\{P_{tpr}, P_{tnr}, P_{ppv}, P_{npv}\}$ remains the same. Thus, a significant change of any P_\star , implies a change in underlying joint distribution (y_t, \hat{y}_t) , or concept. It is worth noting that at every time step t , for any possible (y_t, \hat{y}_t) pair, only two of the four empirical rates in P_\star will change and these two rates are referred to as “influenced by (y_t, \hat{y}_t) ”.

III. CONCEPT DRIFT DETECTION FRAMEWORK

Given the potency of the P_\star (where, $\star \in \{tpr, tnr, ppv, npv\}$) to detect concept drift, the proposed concept drift detection framework uses estimators of the rates in P_\star as test statistics to conduct statistical hypothesis testing at each time step. Specifically, the framework at each time step t conducts statistical tests with the following null and alternative hypotheses:

$$H_0 : \forall \star, P(\text{estimator of } P_\star^{(t-1)}) = P(\text{estimator of } P_\star^{(t)})$$

$$H_A : \exists \star, P(\text{estimator of } P_\star^{(t-1)}) \neq P(\text{estimator of } P_\star^{(t)}).$$

The concept is stable under H_0 and is considered to have drifted if H_0 is rejected. The idea is to compare the statistical significance level of the running test statistic under H_0 at each

time step to the user defined warning (δ_\star) and detection (ϵ_\star) significance levels.

A naïve implementation of the framework (Naïve Four Rates) would be to use $\hat{P}_\star^{(t)}$ (empirical rate of $P_\star^{(t)}$), as the estimators and test statistics. But as shown in Section III-C, there are better estimates of $\hat{P}_\star^{(t)}$.

In the following section, Linear Four Rates (LFR) algorithm will be used to elaborate on the concept drift detection framework. LFR differs from Naïve Four Rates (NFR) in terms of the estimator used. However, both LFR as well as NFR perform better than DDM and DDM-OCI due to the more comprehensive detection framework utilized.

A. Linear Four Rates algorithm (LFR)

1) *Algorithm Outline:* LFR uses modified rates $R_\star^{(t)}$ as the test statistics for $P_\star^{(t)}$. $R_\star^{(t)}$ is a modified version of the empirical rate $\hat{P}_\star^{(t)}$. At each t , $R_\star^{(t)}$ is updated as : $R_\star^{(t)} \leftarrow \eta_\star R_\star^{(t-1)} + (1 - \eta_\star) \mathbf{1}_{\{y_t = \hat{y}_t\}}$ for those empirical rates \star “influenced by (y_t, \hat{y}_t) ”. $R_\star^{(t)}$ is essentially a linear combination of classifier’s previous performance $R_\star^{(t-1)}$ and current performance $\mathbf{1}_{\{y_t = \hat{y}_t\}}$, where η_\star is a time decay factor for weighting the classifier’s performance at current instance. $R_\star^{(t)}$ has been used as a class imbalance detector and as a revised recall test statistic in [9][2]. The probabilistic characteristic of our test statistic R_\star are investigated in § III-A2. The pseudocode of the framework (using $R_\star^{(t)}$ as an estimator of $P_\star^{(t)}$ for required test statistic), is detailed in Algorithm 1.

The three user defined parameters are the time decaying factor (η_\star), warning significance level (δ_\star) and detection significance level (ϵ_\star) for each rate. Time decaying factor is a weight in $[0, 1]$ to evaluate performance of classifier \hat{f} at current instance prediction $\hat{f}(\mathbf{X}_t)$. Given that the detection methodology is conducting hypothesis testing at each time step, δ_\star and ϵ_\star are interpretable statistical significance levels, i.e., type I error (false alarm rate), in standard testing framework. In practice, allowable false warning rate and false detection rate in applications such as quality control of the moving assembly line are guidelines to help the user choose the parameters δ_\star and ϵ_\star . For the fair comparison, η_\star is set to the same value of 0.9 as in [2], for all experiments of this paper. The optimal selection of η_\star is domain dependent and can be pre-learned if necessary.

Theorem 1 in Section III-A2 shows that under the stable concept, $R_\star^{(t)}$ is a geometrically weighted sum of i.i.d Bernoulli random variables, which emphasizes the most recent prediction accuracy and places exponentially decaying weights on the historical prediction accuracies. By taking advantage of this weighting scheme, $R_\star^{(t)}$ is more sensitive to concept drifts, foreshadowing the non-stationarity of classifier’s performance.

Standing on Theorem 1, we are able to overcome the shortcoming of [2] and construct a more reliable running confidence interval for $R_\star^{(t)}$ to control the type-I error ϵ_\star . $R_\star^{(t)}$ is distributed as geometrically weighted sum of Bernoulli random variables. Bhati et. al investigates the closed-form distribution function of $R_\star^{(t)}$ for the special case $P_\star = 0.5$ [10]. However, a closed-form distribution function for other values

Algorithm 1 Linear Four Rates method (LFR)

Input: Data: $\{(\mathbf{X}_t, y_t)\}_{t=1}^{\infty}$ where $\mathbf{X}_t \in \mathbb{R}^d$ and $y_t \in \{0, 1\}$
 Binary classifier $\hat{f}(\cdot)$; Time decaying factors η_{\star} ; Warn significance level δ_{\star} ; Detect significance level ϵ_{\star} .

Output: Detected concept drift time (t_{cd})

- 1: $\hat{P}_{\star}^{(0)} \leftarrow 0.5$, $R_{\star}^{(0)} \leftarrow 0.5$, where $\star \in \{tpr, tnr, ppv, npv\}$ and confusion matrix $C^{(0)} \leftarrow [1, 1; 1, 1]$;
- 2: **for** $t = 1$ to ∞ **do**
- 3: $\hat{y}_t \leftarrow \hat{f}(\mathbf{X}_t)$
- 4: $C^{(t)}[\hat{y}_t][y_t] \leftarrow C^{(t-1)}[\hat{y}_t][y_t] + 1$
- 5: **while** ($\star \in \{tpr, tnr, ppv, npv\}$) **do**
- 6: **if** (\star is influenced by (y_t, \hat{y}_t)) **then**
- 7: $R_{\star}^{(t)} \leftarrow \eta_{\star} R_{\star}^{(t-1)} + (1 - \eta_{\star}) \mathbf{1}_{\{y_t = \hat{y}_t\}}$
- 8: **else**
- 9: $R_{\star}^{(t)} \leftarrow R_{\star}^{(t-1)}$
- 10: **end if**
- 11: **if** ($\star \in \{tpr, tnr\}$) **then**
- 12: $N_{\star} \leftarrow C^{(t)}[0, \mathbf{1}_{\{\star=tpr\}}] + C^{(t)}[1, \mathbf{1}_{\{\star=tpr\}}]$
- 13: $\hat{P}_{\star}^{(t)} \leftarrow \frac{C^{(t)}[\mathbf{1}_{\{\star=tpr\}}, \mathbf{1}_{\{\star=tpr\}}]}{N_{\star}}$
- 14: **else**
- 15: $N_{\star} \leftarrow C^{(t)}[\mathbf{1}_{\{\star=ppv\}}, 0] + C^{(t)}[\mathbf{1}_{\{\star=ppv\}}, 1]$
- 16: $\hat{P}_{\star}^{(t)} \leftarrow \frac{C^{(t)}[\mathbf{1}_{\{\star=ppv\}}, \mathbf{1}_{\{\star=ppv\}}]}{N_{\star}}$
- 17: **end if**
- 18: $\text{warn.bd}_{\star} \leftarrow \text{BoundTable}(\hat{P}_{\star}^{(t)}, \eta_{\star}, \delta_{\star}, N_{\star})$
- 19: $\text{detect.bd}_{\star} \leftarrow \text{BoundTable}(\hat{P}_{\star}^{(t)}, \eta_{\star}, \epsilon_{\star}, N_{\star})$
- 20: **end while**
- 21: **if** (any $R_{\star}^{(t)}$ exceeds warn.bd_{\star} & $\text{warn.time} = 0$) **then**
- 22: $\text{warn.time} \leftarrow t$
- 23: **else if** (no $R_{\star}^{(t)}$ exceeds warn.bd_{\star}) **then**
- 24: $\text{warn.time} \leftarrow 0$
- 25: **end if**
- 26: **if** (any $R_{\star}^{(t)}$ exceeds detect.bd_{\star}) **then**
- 27: $\text{detect.time} \leftarrow t$;
- 28: relearn $\hat{f}(\cdot)$ using $\{(\mathbf{X}_t, y_t)\}_{t=\text{warn.time}}$
- 29: reset $R_{\star}^{(t)}, \hat{P}_{\star}^{(t)}, C^{(t)}$ as done in Step 1
- 30: return $t_{cd} \leftarrow t$
- 31: **end if**
- 32: **end for**

of P_{\star} is unattainable. Alternatively, according to Theorem 1, a reasonable empirical distribution can also be obtained by Monte Carlo simulation for a given P_{\star} and time decaying factor η . The pseudocode for the Monte Carlo sampling procedure is provided in Algorithm 2. As P_{\star} is unknown, \hat{P}_{\star} is used as its surrogate to generate the empirical distribution of $R_{\star}^{(t)}$. Based on the empirical distribution, the lower and upper quantile for the given significance level α , serves as the requisite (warning/detect) bounds. The selection of \hat{P}_{\star} as the best surrogate of P_{\star} , is supported the Lemma 1.

δ_{\star} and ϵ_{\star} denote warning and detection significance levels respectively, where $\delta_{\star} > \epsilon_{\star}$. The corresponding warn.bd and detect.bd are obtained from Monte Carlo simulations as described. The bounds of four rates $\{tpr, tnr, ppv, npv\}$ of the framework, can be independently set based on importance, by having distinct ϵ_{\star} . For instance, in some imbalanced classification tasks, performance of the classifier on the minority class

is a higher priority than on the majority class.

Having computed the bounds, the framework considers that a concept drift is likely to occur and sets the warning signal ($\text{warn.time} \leftarrow t$), when any $R_{\star}^{(t)}$ crosses the corresponding warning bounds (warn.bd) for the first time. If any $R_{\star}^{(t)}$ reaches the corresponding detection bound (detect.bd), the concept drift is affirmed at ($\text{detect.time} \leftarrow t$).

All examples stored between warn.time and detect.time are extracted to relearn a new classifier since the stored examples are considered samples of the new concept. In case the number of stored examples is too few to relearn a reasonable classifier, one will have to wait for sufficient training examples. However, if $R_{\star}^{(t)}$ cross the corresponding warning bounds warn.bd , but fail to reach detect.bd , previous warning flag will be erased. After detecting concept drift, $R_{\star}^{(t)}, \hat{P}_{\star}^{(t)}, C^{(t)}$ are reset to their initial values, so that a new monitoring cycle can restart.

Algorithm 2 Generation of BoundTable in LFR algorithm

Input: Estimate of underlying rate \hat{P} ; Time decaying factor η ; Significance level α ; Number of time steps N_{\star} ; Number of random variables num.of.MC ;

Output: Numeric bound for significance level α .

- 1: **for** $j = 1$ to num.of.MC **do**
- 2: Generate N_{\star} independent Bernoulli random variables $\{I_1, I_2, \dots, I_{N_{\star}}\}$ where $I_i \stackrel{iid}{\sim} \text{Bernoulli}(\hat{P})$
- 3: $R[j] \leftarrow (1 - \eta) \sum_{i=1}^{N_{\star}} \eta^{N_{\star}-i} I_i$
- 4: **end for**
- 5: $\{R[j]\}_{j=1}^{\text{num.of.MC}}$ forms a empirical distribution $\hat{F}(R)$, find α -level quantile as the lower bound $lb \leftarrow \text{quantile}(\hat{F}(R), \alpha)$ and $(1 - \alpha)$ -level quantile as the upper bound $ub \leftarrow \text{quantile}(\hat{F}(R), 1 - \alpha)$

2) *Analysis:* The following theorems investigate the statistical properties of LFR test statistic $R_{\star}^{(t)}$.

Theorem 1: For any \star , $R_{\star}^{(T)}$ is a geometrically weighted sum of Bernoulli random variables, when there is a stable concept up to time T : i.e., $R_{\star}^{(T)} = (1 - \eta_{\star}) \sum_{i=1}^{N_{\star}} \eta_{\star}^{N_{\star}-i} I_i$, where $\{I_i\}_{i=1}^{N_{\star}} \stackrel{iid}{\sim} \text{Bernoulli}(P_{\star})$ and P_{\star} is the underlying rate.

Proof: Among total T time steps, suppose $R_{\star}^{(t)}$ is changed according to line 7 at time step $T_1, \dots, T_{N_{\star}}$ where $T_1 < T_2 < \dots < T_{N_{\star}} \leq T$. Hence,

$$\begin{aligned}
 R_{\star}^{(T)} &= R_{\star}^{(T_{N_{\star}})} = \eta_{\star} R_{\star}^{(T_{N_{\star}-1})} + (1 - \eta_{\star}) \mathbf{1}\{y_{T_{N_{\star}}} = \hat{y}_{T_{N_{\star}}}\} \\
 &= \eta_{\star} [\eta_{\star} R_{\star}^{(T_{N_{\star}-2})} + (1 - \eta_{\star}) \mathbf{1}\{y_{T_{N_{\star}-1}} = \hat{y}_{T_{N_{\star}-1}}\}] \\
 &\quad + (1 - \eta_{\star}) \mathbf{1}\{y_{T_{N_{\star}}} = \hat{y}_{T_{N_{\star}}}\} \\
 &= \eta_{\star}^2 R_{\star}^{(T_{N_{\star}-2})} + \eta_{\star} (1 - \eta_{\star}) \mathbf{1}\{y_{T_{N_{\star}-1}} = \hat{y}_{T_{N_{\star}-1}}\} \\
 &\quad + (1 - \eta_{\star}) \mathbf{1}\{y_{T_{N_{\star}}} = \hat{y}_{T_{N_{\star}}}\} \\
 &= \dots \\
 &= (1 - \eta_{\star}) \sum_{i=1}^{N_{\star}} \eta_{\star}^{N_{\star}-i} \mathbf{1}\{y_{T_i} = \hat{y}_{T_i}\} \\
 &= (1 - \eta_{\star}) \sum_{i=1}^{N_{\star}} \eta_{\star}^{N_{\star}-i} I_i
 \end{aligned}$$

where the last equation hold by the stable concept assumption and all indicators are i.i.d Bernoulli random variables with underlying rate P_* . \blacksquare

Lemma 1: Assume the setting in Theorem 1. Under the stable concept, for any $\star \in \{tpr, tnr, ppv, npv\}$, $\hat{P}_*^{(T)}$ is the unique Uniformly Minimum Variance Unbiased Estimator (UMVUE) of P_* . As $T \rightarrow \infty$, $\hat{P}_*^{(T)}$ is approximately distributed as $\mathcal{N}(P_*, \frac{P_*(1-P_*)}{N_*})$.

Proof: Since $\hat{P}_*^{(t)} = \frac{\sum_{i=1}^{N_*} X_{T_i}}{N_*}$ where X_{T_i} is the Bernoulli random variable realized at time T_i with parameter P_* . $\hat{P}_*^{(T)}$ is an unbiased estimator of P_* . By factorization theorem, $\hat{P}_*^{(t)}$ is a sufficient statistic. Also,

$$\begin{aligned} E(g(\hat{P}_*^{(T)})) &= \sum_{i=0}^{N_*} \binom{N_*}{i} P_*^i (1-P_*)^{N_*-i} g\left(\frac{i}{N_*}\right) \\ &= N_*! (1-P_*)^{N_*} \sum_{i=0}^{N_*} \frac{g(i/N_*)}{i!(N_*-i)!} \left(\frac{P_*}{1-P_*}\right)^i \end{aligned}$$

If $E(g(\hat{P}_*^{(T)})) = 0 \ \forall P_*$, it implies $g\left(\frac{i}{N_*}\right) = 0 \ \forall i$ because $E(g(\hat{P}_*^{(T)}))$ is a polynomial of $\frac{P_*}{1-P_*}$. Thereby $P(g(\hat{P}_*^{(T)}) = 0) = 1$ and $\hat{P}_*^{(T)}$ is a complete sufficient statistic by definition. By Lehmann-Scheffe Theorem, $\hat{P}_*^{(T)}$ is the unique UMVUE. \blacksquare

The complexity of Linear Four Rates (LFR) detection algorithm is $O(1)$ at each time step (t). The LFR algorithm can be optimized by using a *BoundTable* precomputed by Algorithm 2 before the start of detection framework. The 4 dimensional *BoundTable* with varying input $(\hat{P}, \eta, \delta, N_*)$ can itself be precomputed before running Algorithm 1. observer can find a closest \hat{P} to $\hat{P}_*^{(t)}$ during monitoring process and look up its lower bound and upper bound from *BoundTable*. Thus, LFR algorithm takes $O(1)$ to test drift occurrence at each time point and suits with streaming environment.

B. Naïve Four Rates algorithm (NFR)

For the purpose of comparison, this section details the characteristics of a naïve implementation of the proposed framework that uses $\hat{P}_*^{(t)}$ as the test statistic. A benefit of choosing this test statistic, is that there exists a closed-form distribution as shown in Lemma 1. Using the same strategy of LFR algorithm, NFR algorithm monitors the four rates $\hat{P}_*^{(t)}$ sequentially. At each time stamp, for each rate, hypothesis testing is done with null distribution $N(P_*, \frac{P_*(1-P_*)}{N_*})$ and the warning / detection alarms set when $\hat{P}_*^{(t)}$ exceeds the expected bounds.

The main difference with respect to LFR is the estimation of P_* used to find null distribution. LFR algorithm uses $\hat{P}_*^{(t)}$ as a surrogate of unknown P_* while NFR algorithm uses $\bar{P}_*^{(t)}$, where $\bar{P}_*^{(t)}$ is a running average of all previous $\hat{P}_*^{(t)}$. This update rule allows old prediction performance contributes more to the estimate of P_* and recent predictions contributes less.

Thus, $\bar{P}_*^{(t)}$ is more robust in terms of estimating the underlying P_* when concept drift occurs. Additionally, $\bar{P}_*^{(t)}$ is still a MSE-consistent estimator under the stable concept presented in Lemma 2.

Lemma 2: Assume the setting in Theorem 1. Under the stable concept up to T , for any $\star \in \{tpr, tnr, ppv, npv\}$, $\bar{P}_*^{(T)}$ in NFR algorithm is a MSE-consistent estimator of P_* .

Proof: Among total T time steps, suppose $\hat{P}_*^{(t)}$ is changed at time step T_1, \dots, T_{N_*} where $T_1 < T_2 < \dots < T_{N_*} \leq T$. Hence,

$$\begin{aligned} \bar{P}_*^{(T)} &= \bar{P}_*^{(T_{N_*})} = \frac{1}{N_*} \sum_{i=1}^{N_*} \hat{P}_*^{(T_i)} \\ &= \frac{1}{N_*} \left[\sum_{n=1}^{N_*} \frac{1}{n} \sum_{i=1}^n \mathbf{1}\{y_{T_i} = \hat{y}_{T_i}\} \right] \\ &= \frac{1}{N_*} \left[\sum_{i=1}^{N_*} \sum_{j=i}^{N_*} \frac{1}{j} \mathbf{1}\{y_{T_i} = \hat{y}_{T_i}\} \right]. \end{aligned}$$

By IID assumption of indicators, we obtain

$$\mathbb{E}(\bar{P}^{(T)}) = \frac{1}{N_*} \left[\sum_{i=1}^{N_*} \sum_{j=i}^{N_*} \frac{1}{j} P_* \right] = P_*$$

and

$$\begin{aligned} \text{VAR}(\bar{P}^{(T)}) &= \frac{1}{N_*^2} \left[\sum_{i=1}^{N_*} \left(\sum_{j=i}^{N_*} \frac{1}{j} \right)^2 P_*(1-P_*) \right] \\ &\leq \frac{\left(\sum_{j=1}^{N_*} \frac{1}{j} \right)^2}{N_*} P_*(1-P_*) \\ &\leq \frac{(\log N_*)^2}{N_*} P_*(1-P_*) \xrightarrow{T \rightarrow \infty} 0 \end{aligned}$$

where the last limit hold by the fact that $N_* \rightarrow \infty$ as $T \rightarrow \infty$. Thus, as $\mathbb{E}(\bar{P}_*^{(T)}) - P_* = 0$ and $\text{VAR}(\bar{P}^{(T)}) \rightarrow 0$, $\bar{P}^{(T)}$ is a MSE-consistent estimator. \blacksquare

C. Comparison between NFR and LFR

To empirically compare the test statistics of NFR and LFR, we use Figure 1 to illustrate a single run of both LFR and NFR algorithm on the same synthetic streaming data. It is clear that the test statistic $R_*^{(t)}$ in LFR algorithm has a larger variance than $\hat{P}_*^{(t)}$ for each rate. LFR algorithm reports an earlier detection at $t = 5167$ (true detection point t=5000) when compared to NFR in this run, even though $\epsilon_*^{(LFR)} < \epsilon_*^{(NFR)}$. This observation matches well with the rationale of constructing $R_*^{(t)}$, described in §III-A1, to gain detection sensitivity through introducing large variances. To rigorously compare detection performance of $R_*^{(t)}$ and $\hat{P}_*^{(t)}$, more investigations are provided below.

Power characteristics of two competing test statistics $R_*^{(t)}$ (LFR) and $\hat{P}_*^{(t)}$ (NFR), are compared empirically on synthetic data. Power estimates of $R_*^{(t)}$ and $\hat{P}_*^{(t)}$ against varying time lag k and q_* are presented in Figure 2. Figure 2 indicates that neither $R_*^{(t)}$ nor $\hat{P}_*^{(t)}$ dominates all the time because $R_*^{(t)}$ (red

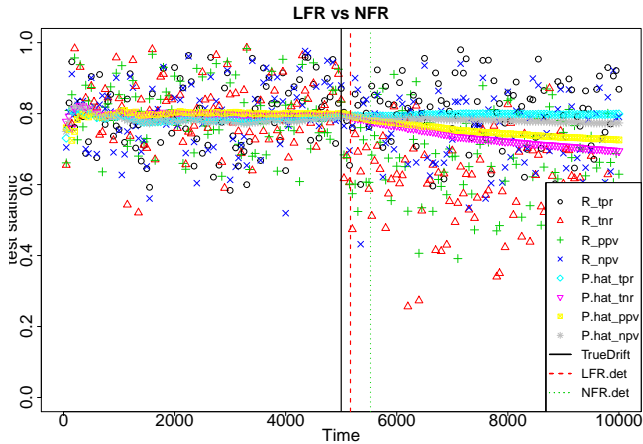


Fig. 1. A single run of LFR and NFR on the same synthetic streaming data. Black, red and green vertical lines are the 'true drift time', LFR detection and NFR detection time respectively. Four colored dots (black, red, green, blue) are running $R_{\star}^{(t)}$ and four colored horizontal lines (indigo, pink, yellow, grey) are running $\hat{P}_{\star}^{(t)}$ where $\star \in \{tpr, tnr, ppv, npv\}$.

surface) achieves a larger statistical power when the time lag K is small but a smaller power when K is large. This is because the update rule line 7 enables the estimator $R_{\star}^{(t)}$ to shift from p_{\star} to q_{\star} at an exponential rate which leads the power dominance in a short lag. The price is that limiting distributions of $R_{\star}^{(t)}$ under both null and alternative have larger variances than $\hat{P}_{\star}^{(t)}$ and thus limiting power, when K is large and $|p_{\star} - q_{\star}|$ is small, is degraded.

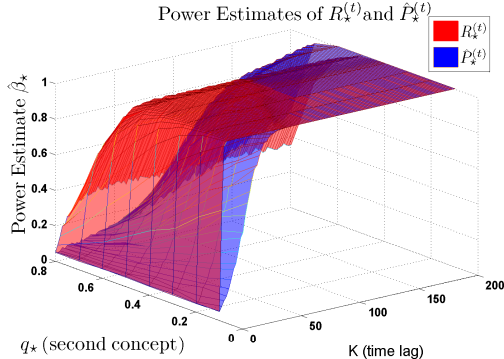


Fig. 2. Power comparison between $R_{\star}^{(t)}$ and $\hat{P}_{\star}^{(t)}$ where null distribution is at $t = M$ and alternative distribution is at $t = M + k$. $M = 1000$, $1 \leq k \leq K$ where $K = 200$ is the maximal time lag. The underlying rate is drifted from $p_{\star} = 0.9$ to q_{\star} where $0.1 \leq q_{\star} \leq 0.8$.

In order to compare sensitivities of $R_{\star}^{(t)}$ and $\hat{P}_{\star}^{(t)}$ with regard to detecting concept drift in more general settings, we used $\Delta\beta = \hat{\beta}_{R_{\star}^{(t)}} - \hat{\beta}_{\hat{P}_{\star}^{(t)}}$. The result is illustrated in Figure 3. Except when, $p_{\star} = q_{\star}$, we see that for any fixed pair of (p_{\star}, q_{\star}) , $\Delta\beta > 0$ when K is small and $\Delta\beta \leq 0$ when K is large. This is because $\Delta\beta$ decreases, as time lag K increases. This suggests that LFR is preferable if earlier detection is highly desired. The alarms are more likely to be triggered in the earliest time after the occurrence of concept drift. Earlier detection allows observer to adjust the model and avoid costs of incorrect predictions immediately. On the other hand, if observers are only concerned with detecting the occurrence of drift in the data stream but unconcerned with its detection promptness, then NFR algorithm provides a higher power

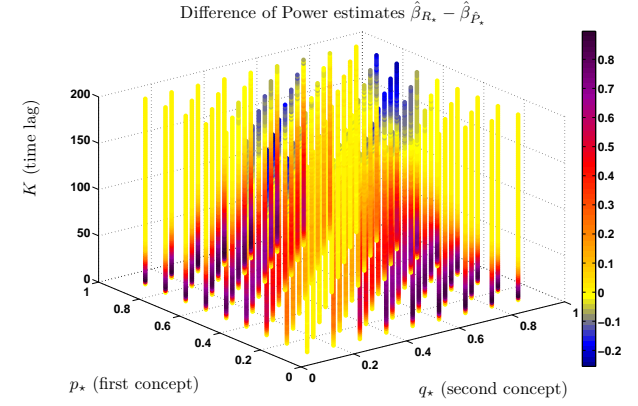


Fig. 3. Power difference $\Delta\beta = \hat{\beta}_{R_{\star}^{(t)}} - \hat{\beta}_{\hat{P}_{\star}^{(t)}}$ along the time lag K in different combinations of concept change from p_{\star} to q_{\star} .

test statistic to detect the drift. This is because $\hat{P}_{\star}^{(t)} \rightarrow q_{\star}$ with convergence rate $O(\frac{1}{K})$. In the long run, as $K \rightarrow \infty$, $\hat{P}_{\star}^{(t)} \rightarrow q_{\star}$ implies that $\beta_{\hat{P}_{\star}^{(t)}} \rightarrow 1$.

To guide the selection between LFR and NFR, Figure 4 is a heatmap of limiting power estimates on all (p_{\star}, q_{\star}) pairs using $K = 200$. We can see that $\hat{\beta}_{R_{\star}}$ is already close to 1 for $K = 200$, when p_{\star} and q_{\star} are significantly different.

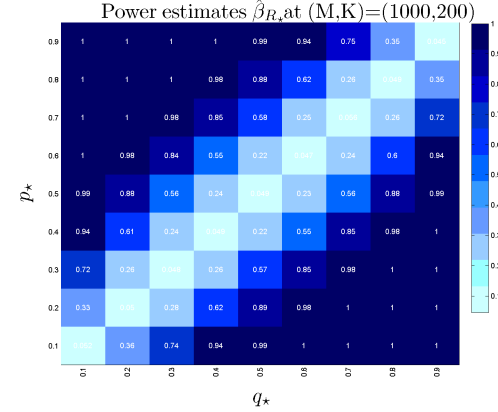


Fig. 4. Heatmap of Power estimates $\hat{\beta}_{R_{\star}}$.

IV. EXPERIMENTS

In this section, we compared the detection performance of LFR to NFR, DDM and DDM-OCI approaches using both synthetic data and public datasets. We considered 3 simulated class-balance datasets, 3 simulated class-imbalance datasets and 4 public datasets to demonstrate LFR algorithm performs well across various types of concept drifts, including those where the baseline performs poorly.

To generalize the performance and evaluate confidences of algorithms, for each dataset, the order of (\mathbf{X}_t, y_t) pairs within each concept are permuted to create 100 bootstrapped dataset streams. Each stream is fed to all detection algorithms to obtain single-run detections for each method. To illustrate the accuracy of the prediction, we use overlapped histograms to visualize the distribution of detection points obtained from the concept drift detection models across the 100 runs. To avoid

| Parameters | Detect Sig. | Warn Sig. | Decay |
|------------|------------------------|----------------------|----------------|
| LFR | $\epsilon_* = 1/100K$ | $\delta_* = 1/100$ | $\eta_* = 0.9$ |
| NFR | $\epsilon_* = 1/1K$ | $\delta_* = 0.025$ | $\eta_* = 0.9$ |
| DDM | $\alpha_{detect} = 3$ | $\alpha_{warn} = 2$ | $\eta_* = 0.9$ |
| DDM-OCI | $\alpha_{detect} = 20$ | $\alpha_{warn} = 10$ | $\eta_* = 0.9$ |

TABLE I. PARAMETER SETTINGS USED IN SECTION IV-A EXPERIMENTS

| Para. | SEA | HYPRLPN. | USENET1&2 |
|---------|--|--|--|
| LFR | $\epsilon_* = 1/10K$ $\delta_* = 1/100$ | $\epsilon_* = 1/10K$ $\delta_* = 1/100$ | $\epsilon_* = 1/10K$ $\delta_* = 1/100$ |
| NFR | $\epsilon_* = 1/1K$ $\delta_* = 0.025$ | $\epsilon_* = 1/1K$ $\delta_* = 0.025$ | $\epsilon_* = 1/1K$ $\delta_* = 0.025$ |
| DDM | $\alpha_{detect} = 3$ $\alpha_{warn} = 2$ | $\alpha_{detect} = 3$ $\alpha_{warn} = 2$ | $\alpha_{detect} = 3$ $\alpha_{warn} = 2$ |
| DDM-OCI | $\alpha_{detect} = 20$ $\alpha_{warn} = 10$ | $\alpha_{detect} = 30$ $\alpha_{warn} = 10$ | $\alpha_{detect} = 3$ $\alpha_{warn} = 2$ |

TABLE II. PARAMETER SETTINGS USED IN SECTION IV-B EXPERIMENTS

redundancy, we present 6 histograms out of 10 experiments and remaining ones are similar.

The best algorithm will have the minimal number of false alarms and maximal number of early detections, whereas poor algorithms give large number of false alarms, missing or severely delayed true detections. A summary of the counts of correct detections at true drift timestamp and counts of false detections during false detection period for the simulated and public datasets are provided in Tables IV and Table V. False detection period refers to the period preceding the data points that belong to the new concept. For the synthetically generated datasets in Section IV-A, there were two concepts spanning the T data points, such that the false detection period is defined as $[0, T/2)$. For the datasets specified in Section IV-B, if there were more than two concepts, the false detection period corresponds to the range from the concept midway up to the next true drift point. Each bin in the histograms shown below correspond to 200 time steps in Section IV-A and dataset-dependent in §IV-B. Other parameter settings of detection algorithms are summarized in Table I and II. As shown below, LFR consistently outperformed the baseline approaches. When compared to NFR, LFR correctly identifies more true drift points with higher probability and smaller number of false alarms even with a smaller ϵ_* .

A. Synthetic Data

Numerous experiments were run on synthetic data, covering the various types of concept drift. In each synthetic experiment, a data stream of pairs $\{(y_t, \hat{y}_t)\}_{t=1}^T$ with one change-point at $T/2$ is generated by sampling from two confusion probability matrices $CP^{(1)}$ and $CP^{(2)}$. The two concepts are characterized by $CP^{(1)}$ and $CP^{(2)}$, respectively and the type of drift is determined by particular settings of $(CP^{(1)}, CP^{(2)})$. For example, to generate a balanced stream of pairs $\{(y_t, \hat{y}_t)\}_{t=1}^T$ representing the scenario that overall accuracy of classifier drops but P_{tpr} remains constant, we chose $CP^{(1)} = \begin{pmatrix} 0.4 & 0.1 \\ 0.1 & 0.4 \end{pmatrix}$ and $CP^{(2)} = \begin{pmatrix} 0.3 & 0.1 \\ 0.2 & 0.4 \end{pmatrix}$. The objective of detection algorithms is to identify the change-point $T/2$. The more challenging and interesting scenarios are discussed below.

1) *Balanced Dataset*: In balanced datasets, $P(y_t = 0) = P(y_t = 1)$ is required in underlying data generation. Class-

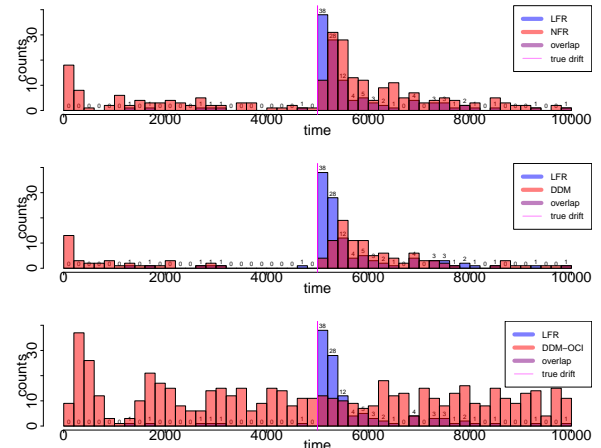


Fig. 5. Overlapping histograms comparing detection timestamps on Balance1 dataset.

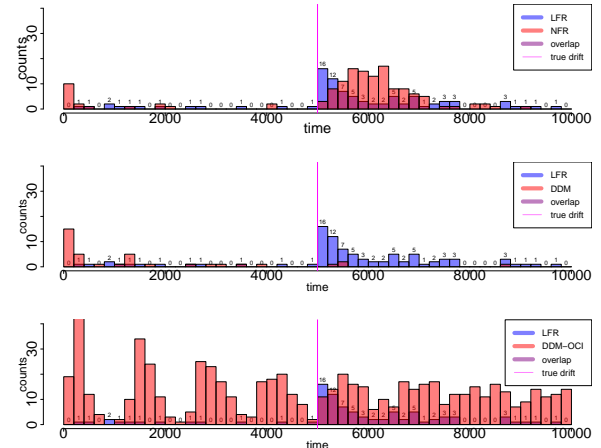


Fig. 6. Overlapping histograms comparing detection timestamps on Balance2 dataset.

balance data are the most typical scenario in classification task and hence investigated with following three representative experiments.

- Balance1: Overall accuracy of classifier drops but P_{tpr} remains constant with $CP^{(1)}$ and $CP^{(2)}$ above.
- Balance2: Gradual drift in which overall accuracy $(1 - P_{error})$ remains the same with $CP^{(1)} = \begin{pmatrix} 0.35 & 0.05 \\ 0.15 & 0.45 \end{pmatrix}$, $CP^{(2)} = \begin{pmatrix} 0.4 & 0.1 \\ 0.1 & 0.4 \end{pmatrix}$.
- Balance3: Overall accuracy $(1 - P_{error})$ increases and P_{tpr} remains unchanged with $CP^{(1)} = \begin{pmatrix} 0.3 & 0.2 \\ 0.2 & 0.4 \end{pmatrix}$, $CP^{(2)} = \begin{pmatrix} 0.4 & 0.2 \\ 0.1 & 0.3 \end{pmatrix}$.

2) *Imbalanced Dataset*: For imbalanced datasets, we used the same data generation mechanism as balanced case but make $P(y_t = 0)$ and $P(y_t = 1)$ imbalanced. We considered the following three interesting cases given many attentions to in real applications.

- Imbalance1: From class balance dataset to class imbalance dataset with $CP^{(1)} = \begin{pmatrix} 1/3 & 1/6 \\ 1/6 & 1/3 \end{pmatrix}$ and $CP^{(2)} = \begin{pmatrix} 1/2 & 1/4 \\ 1/4 & 1/2 \end{pmatrix}$.

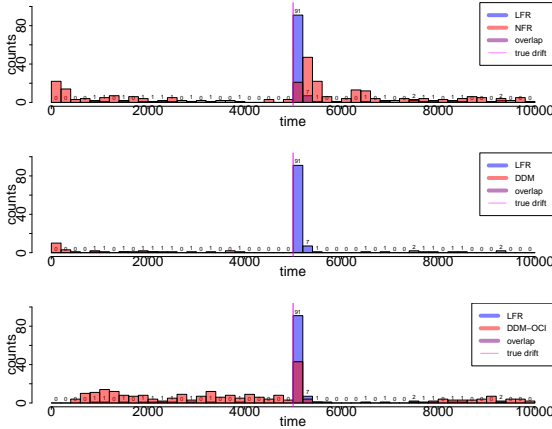


Fig. 7. Overlapping histograms comparing detection timestamps on Imbalance1 dataset.

$\begin{pmatrix} 13/15 & 1/30 \\ 1/30 & 1/30 \end{pmatrix}$. Without loss of generality, let $y = 1$ be the minority class. It is also noteworthy that P_{tpr} and P_{ppv} are unchanged after drift occurrence. Hence, many detectors in imbalance data learning society, using F1 score as a measure to monitor classifier performance, is unable to alarm this type of drift. However, Fig. 7 shows that LFR performs very well by dominating both high early detection rate and trivial false alarms. Besides, DDM and DDM-OCI has no detection after changepoint due to the increment of $(1 - P_{error})$ and P_{tpr} , respectively.

- (ii) Imbalance2: The class ratio and P_{error} remain unchanged but P_{tpr} decreases with $CP^{(1)} = \begin{pmatrix} 0.65 & 0.05 \\ 0.15 & 0.15 \end{pmatrix}$ and $CP^{(2)} = \begin{pmatrix} 0.75 & 0.15 \\ 0.05 & 0.05 \end{pmatrix}$.
- (iii) Imbalance3: All P_{tpr}, P_{ppv} and $1 - P_{error}$ decreases. Though class ratio remains the same, both F1-score and overall accuracy decreases. Two conditional probability matrices are selected as $CP^{(1)} = \begin{pmatrix} 0.6 & 0.15 \\ 0.15 & 0.1 \end{pmatrix}$ and $CP^{(2)} = \begin{pmatrix} 0.6 & 0.15 \\ 0.15 & 0.1 \end{pmatrix}$.

B. Public Datasets

All detection algorithms are evaluated on four public datasets used in literature. Without loss of generality, we chose the Support Vector Machine (SVM)[11] with an RBF Kernel as the classifier \hat{f} , because all detection algorithms are independent of type of classifiers. Misclassification of the minority class is penalized 100 times more than the majority class. If a potential concept drift is reported by the algorithm, examples from the new concept will be stored to retrain a new SVM classifier \hat{f}_{new} , adapted with new concept. Specifically, 1000 examples are used for retraining on SEA and Rotating Hyperplane datasets; 100 examples are used for retraining on USENET1 and USENET2 datasets.

1) *Datasets*: SEA Concepts dataset is used in [12]. The dataset is available at <http://www.liaad.up.pt/kdus/products/datasets-for-concept-drift>, and is widely used as a testbed by concept drift detection algorithms. Rotating Hyperplane dataset

| Dataset | T | True Drift Time | dimensions (d) |
|---------|-------|------------------------------|--------------------|
| SEA | 60000 | $\{15000 \times i\}_{i=1}^3$ | 3 |
| HYPER. | 90000 | $\{10000 \times i\}_{i=1}^1$ | 10 |
| USENET1 | 1500 | $\{300 \times i\}_{i=1}^5$ | 100 |
| USENET1 | 1500 | $\{300 \times i\}_{i=1}^5$ | 100 |

TABLE III. KEY FEATURES OF DATASETS.

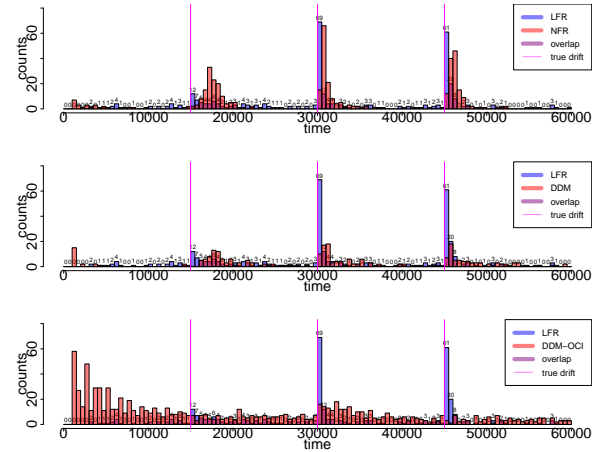


Fig. 8. Overlapping histograms comparing detection timestamps on SEA

is created by [13]. The dataset and specific (k, t) pairs of each concept are available at <http://www.win.tue.nl/~mpechen/data/DriftSets/>. USENET1 and USENET2 datasets, used in [14], are available at http://mlkd.csd.auth.gr/concept_drift.html. They are stream collections of messages from different newsgroups (e.g. medicine, space, baseball) to a user. The difference between USENET1 and USENET2 is the magnitude of drift. The user in USENET1 has a sharper topic shift than the one in USENET2.

All above datasets are in form of $\{\mathbf{X}_t, y_t\}_{t=1}^T$ and their key features are summarized in Table III.

2) *Evaluation*: In SEA Concepts Dataset experiment, Fig. 8 shows that LFR dominates other three approaches in terms of early detections and fewer false or delayed detections.

Fig. 9 shows that LFR has a dominant performance on the

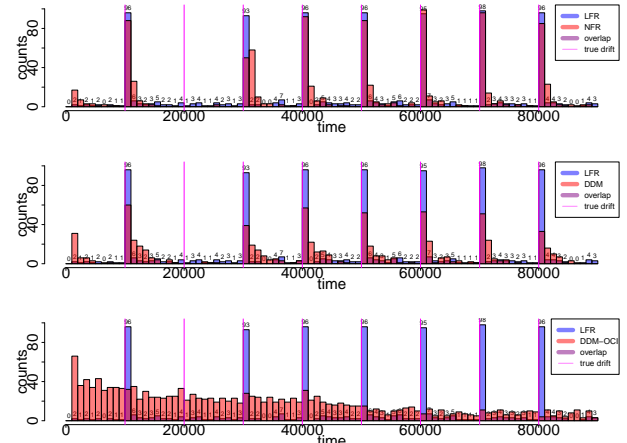


Fig. 9. Overlapping histograms comparing detection timestamps on HYPER-PLANE

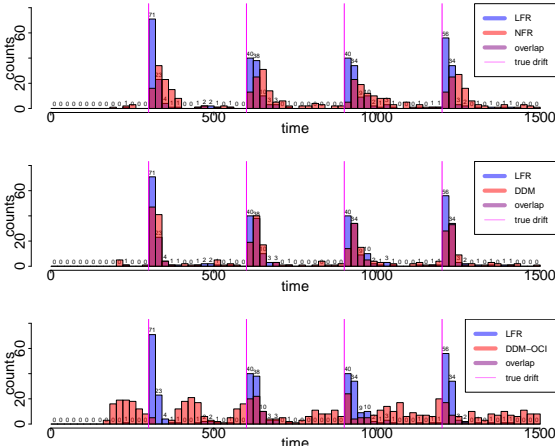


Fig. 10. Overlapping histograms comparing detection timestamps on USENET1

| Metric | LFR | NFR | DDM | DDM-OCI |
|------------|-----|-----|-----|---------|
| Balance1 | 38 | 12 | 4 | 12 |
| Balance2 | 16 | 3 | 0 | 11 |
| Balance3 | 25 | 4 | 0 | 3 |
| Imbalance1 | 95 | 59 | 0 | 4 |
| Imbalance2 | 91 | 21 | 0 | 43 |
| Imbalance3 | 95 | 38 | 36 | 39 |
| SEA | 142 | 29 | 17 | 26 |
| HYPRPLN | 671 | 598 | 345 | 149 |
| USENET1 | 207 | 47 | 108 | 66 |
| USENET2 | 3 | 17 | 3 | 21 |

TABLE IV. THE COUNT (SUM) AT (MULTIPLE) TRUE DRIFT POINT CORRECTLY DETECTED FOR SIMULATED (PUBLIC) DATASETS.

Rotation Hyperplane Dataset experiment. At the second true drift time point, the underlying concept change is very minor. Hence the drift is neglected by all detection algorithms.

In USENET1 dataset experiment, Fig. 10 indicates LFR dominates other approaches and all drift points are alarmed. Similarly, in USENET2 dataset experiment, LFR also outperforms other approaches but detections are delayed with longer time lag. The decrement of superiority of LFR, from USENET1 to USENET2 is due to decrements of magnitude of concept drifts.

As summarized in Table IV, LFR fared best in terms of recall of true change point detection across the various datasets. Equally importantly, LFR had the highest precision with regard to detecting change points by producing the least amount of false detection and delayed detection (Table V).

| Metric | LFR | NFR | DDM | DDM-OCI |
|------------|-----|-----|-----|---------|
| Balance1 | 6 | 77 | 36 | 304 |
| Balance2 | 13 | 19 | 33 | 339 |
| Balance3 | 18 | 54 | 11 | 219 |
| Imbalance1 | 18 | 81 | 16 | 259 |
| Imbalance2 | 10 | 91 | 23 | 165 |
| Imbalance3 | 9 | 86 | 55 | 204 |
| SEA | 72 | 32 | 54 | 658 |
| HYPRPLN | 84 | 56 | 73 | 826 |
| USENET1 | 12 | 50 | 43 | 322 |
| USENET2 | 43 | 80 | 65 | 272 |

TABLE V. THE COUNT (SUM) AT (MULTIPLE) FALSE DETECTION FOR THE SIMULATED (PUBLIC) DATASETS

V. CONCLUSION

The paper presents a concept drift detection framework (LFR) for detecting the occurrence of a concept drift and identifies the data points that belong to the new concept. The versatility of LFR allows it to work with both batch and stream datasets, imbalanced data sets and it uses user-specified parameters that are intuitively comprehensible, unlike other popular concept drift detection approaches. LFR significantly outperforms existing benchmark approaches in terms of early detection of concept drifts, high detection rate and low false alarm rate across the types of concept drifts.

REFERENCES

- [1] J. Gama, P. Medas, G. Castillo, and P. Rodrigues, "Learning with drift detection," in *Advances in Artificial Intelligence–SBIA 2004*. Springer, 2004, pp. 286–295.
- [2] S. Wang, L. L. Minku, D. Ghezzi, D. Caltabiano, P. Tino, and X. Yao, "Concept drift detection for online class imbalance learning," in *Neural Networks (IJCNN), The 2013 International Joint Conference on*. IEEE, 2013, pp. 1–10.
- [3] M. Baena-García, J. del Campo-Ávila, R. Fidalgo, A. Bifet, R. Gavaldà, and R. Morales-Bueno, "Early drift detection method," 2006.
- [4] D. K. Antwi, H. L. Viktor, and N. Japkowicz, "The perfsim algorithm for concept drift detection in imbalanced data," in *Data Mining Workshops (ICDMW), 2012 IEEE 12th International Conference on*. IEEE, 2012, pp. 619–628.
- [5] R. Klinkenberg and T. Joachims, "Detecting concept drift with support vector machines," in *Proceedings of the Seventeenth International Conference on Machine Learning*. Morgan Kaufmann Publishers Inc., 2000, pp. 487–494.
- [6] D. S. Matteson and N. A. James, "A nonparametric approach for multiple change point analysis of multivariate data," *Journal of the American Statistical Association*, vol. 109, no. 505, pp. 334–345, 2014.
- [7] X. Song, M. Wu, C. Jermaine, and S. Ranka, "Statistical change detection for multi-dimensional data," in *Proceedings of the 13th ACM SIGKDD international conference on Knowledge discovery and data mining*. ACM, 2007, pp. 667–676.
- [8] A. Dries and U. Rückert, "Adaptive concept drift detection," *Statistical Analysis and Data Mining*, vol. 2, no. 5–6, pp. 311–327, 2009.
- [9] S. Wang, L. L. Minku, and X. Yao, "A learning framework for online class imbalance learning," in *Computational Intelligence and Ensemble Learning (CIEL), 2013 IEEE Symposium on*. IEEE, 2013, pp. 36–45.
- [10] D. Bhati, P. Kgosi, and R. N. Rattihalli, "Distribution of geometrically weighted sum of bernoulli random variables," *Applied Mathematics*, vol. 2, p. 1382, 2011.
- [11] D. Meyer, "Support vector machines."
- [12] W. N. Street and Y. Kim, "A streaming ensemble algorithm (sea) for large-scale classification," in *Proceedings of the seventh ACM SIGKDD international conference on Knowledge discovery and data mining*. ACM, 2001, pp. 377–382.
- [13] W. Fan, "Systematic data selection to mine concept-drifting data streams," in *Proceedings of the tenth ACM SIGKDD international conference on Knowledge discovery and data mining*. ACM, 2004, pp. 128–137.
- [14] I. Katakis, G. Tsoumakas, and I. P. Vlahavas, "An ensemble of classifiers for coping with recurring contexts in data streams." 2008.